Korean J. Chem. Eng., 34(12), 3220-3225 (2017)
DOI: 10.1007/s11814-017-0237-4

pISSN: 0256-1115
eISSN: 1975-7220

Preparation of WO_3, $BiVO_4$ and reduced graphene oxide composite thin films and their photoelectrochemical performance

Sang-Hyeok Yoon*, Dong-Wha Park, and Kyo-Seon Kim*,†**

*Department of Chemical Engineering, Kangwon National University,
1 Kangwondaehak-gil, Chuncheon-si, Kangwon-do 24341, Korea
**Department of Chemical Engineering, Inha University, 100 Inharo, Nam-gu, Incheon 22212, Korea
(*Received 16 July 2017 • accepted 21 August 2017*)

Abstract−Various thin films for photoelectrochemical (PEC) water splitting were prepared and their PEC performance was tested. The precursor solutions for WO_3 and $BiVO_4$ photocatalysts were synthesized by solution processes, and the graphene oxide (GO) was prepared by Tour's method and was calcined and converted to reduced graphene oxide (rGO). The composite photocatalyst thin films of WO_3, $BiVO_4$, $WO_3/BiVO_4$ and $WO_3/BiVO_4$-rGO were prepared on fluorine doped tin oxide glass by spin coating and calcination processes and the PEC performances were analyzed for those photocatalyst layers. The controlled $WO_3/BiVO_4$ heterojunction layer showed better PEC performance than the WO_3 or $BiVO_4$ single layer by the combined effects of photocatalysts. The $WO_3/BiVO_4$-rGO film with the optimum concentration of rGO showed a noticeable increase in photocurrent density because of the increased electrical conductivity by rGO and reduced recombination rate in $BiVO_4$ layer.

Keywords: Production of Hydrogen, PEC Water Splitting, Heterojunction Photocatalyst Layers, Reduced Graphene Oxide (rGO), $WO_3/BiVO_4$-rGO Thin Film

INTRODUCTION

Hydrogen is one of the important future alternative energies to overcome the energy crisis. Photoelectrochemical (PEC) water splitting has been considered as one of promising methods to generate hydrogen and the photocatalysts in PEC water splitting make electron-hole pairs by photoexcitation. The photogenerated electron-hole pairs are transferred to active sites of electrodes and split the water into hydrogen and oxygen by redox reactions. For the effective PEC water splitting, the photocatalysts need to have the band-gap excited efficiently by the energy of solar light and the effective transport properties of photogenerated electron-hole pairs [1]. TiO_2 has been the most popular photocatalyst for the research of PEC water splitting, but it can utilize only 4% of sunlight due to its relatively large band gap of about 3.0-3.2 eV [2]. WO_3 has a lower band gap of 2.8 eV and is believed to be more appropriate photocatalyst to utilize visible solar light [2]. Instead, its level of conduction band is lower than the reduction potential required for water splitting [3-5], and the bias voltage needs to be applied to reach the reduction potential. Although $BiVO_4$ does not have a suitable position of conduction band for water splitting either [5], it has several advantages as a photocatalyst, because it has narrower band gap (2.4 eV) and high stability, is inexpensive and environmentally benign, and it can be synthesized by several facile methods. But $BiVO_4$ also has the disadvantage of high recombination rate between electrons and holes, resulting in low effective photocurrent density [6]. Recently, many research groups have attempted to improve the photocatalytic activities by nanostructure control [7-9], metal or nonmetal ion doping [4,10-12] and heterojunction structures [13-15].

Heterojunction thin films combining two different photocatalysts are proposed as the plausible method to overcome the abovementioned disadvantages of photocatalysts and to improve the PEC water splitting efficiency [16-19]. Because all photocatalysts have different band gap positions of their own, photogenerated electrons can be separated from holes in heterojunction thin film more efficiently by the proper choice of photocatalysts, and the electrons and holes can be transferred to the active sites more effectively without the recombination reactions and, as a result, the PEC performance can be improved. When WO_3 and $BiVO_4$ are combined in heterojunction thin film, the photogenerated electrons in $BiVO_4$ layer can be transferred to WO_3 layer, because the conduction band of WO_3 is lower than $BiVO_4$, but the holes cannot be transferred to WO_3 layer because the valence band of WO_3 is lower than $BiVO_4$ and the electrons and holes are separated more efficiently without recombination reactions [14].

Many research groups have proved that the graphene has some positive effects on the activities of photocatalysts ($BiVO_4$ [6], TiO_2 [20], ZnO [21], WO_3 [22], Fe_2O_3 [23]). Graphene also has high electrical conductivity [24] and, by combining the photocatalyst with graphene, the photo-excited electrons in photocatalyst can be separated from holes more easily and, as a result, the PEC water splitting efficiency can be improved significantly [6,20-23]. Although $BiVO_4$ has several advantages as photocatalyst, it could not generate high photocurrent density due to high recombination rate, but a notable enhancement in the current density was obtainable through the addition of graphene in $BiVO_4$ electrodes [6].

†To whom correspondence should be addressed.
E-mail: kkyoseon@kangwon.ac.kr

Separate studies on PEC performance with $WO_3/BiVO_4$ heterojunction or photocatalyst-rGO composite have been done, but there has been no study on the combined effects of WO_3, $BiVO_4$ and rGO yet. In this study, we prepared several composite photocatalyst thin films of WO_3, $BiVO_4$, and rGO on fluorine doped tin oxide (FTO) glass and compared the PEC performance of those photocatalyst layers (WO_3, $BiVO_4$, $WO_3/BiVO_4$ and $WO_3/BiVO_4$-rGO) for the first time. WO_3 and $BiVO_4$ are well known to have high visible light activity and stability. We prepared the heterojunction of WO_3 and $BiVO_4$ by solution processes and the rGO was added to $BiVO_4$ layer to supplement the poor electrical conductivity of $BiVO_4$. The properties of prepared thin films were analyzed by UHR-SEM (Ultra high resolution scanning electron microscope), HRXRD (High resolution X-ray diffractometer) and XPS (X-ray photoelectron spectroscopy). The PEC performance of prepared thin films was measured by PEC cell and analyzed.

EXPERIMENTAL

1. Preparation of GO

The GO was prepared based on Tour's method, which is safer, simpler and more environmentally benign to get high degree of oxidation than Hummer's method [25]. First, 360 ml of sulfuric acid (H_2SO_4, 98% GR, Daejung) and 40 ml of phosphoric acid (H_3PO_4, 85% GR, Daejung) were mixed. Next, the prepared solution was poured into the mixture of 3 g of graphite powder (CP, Daejung) and 18 g of potassium permanganate ($KMnO_4$, 99.3% GR, Junsei) and intensively stirred at 50 °C for 12 hr. Then, hydrogen peroxide solution (H_2O_2, 30-35.5% GR, Wako) was added to the mixed solution to terminate the oxidation reaction. The prepared GO was exfoliated by sonication and was centrifuged and washed using dilute hydrochloric acid and acetone solution. The sufficient washing was confirmed by the precipitation reaction with barium chloride and the titration with pH paper.

2. Preparation of Precursor Solution for Photocatalyst Thin Films

The WO_3 precursor solution was prepared by mixing 5 g of ammonium tungsten oxide hydrate ($(NH4)_6W_{12}O_{39}{\cdot}xH_2O$, Alfa Aesar), 2.5 g of PVP (polyvinylpyrrolidone, K30, CP, Daejung) and 25 ml of distilled water in sonication bath for about 30 min to dissolve the solid materials completely.

To prepare the $BiVO_4$ precursor solution, we made two kinds of solutions at first: solution 1 was made by dissolving bismuth(III) nitrate pentahydrate ($Bi(NO_3)_3{\cdot}5H_2O$, ≥98.0% ACS reagent, Sigma-Aldrich) in acetic acid (CH_3COOH, 99.9% SSG, Wako) with the ratio of 25 mg : 1 ml; solution 2 by dissolving vanadyl acetylacetonate ($VO(C_5H_7O_2)_2$, 98%, Aldrich) in acetylacetone ($C_5H_8O_2$, 99% EP, Daejung) with the ratio of 260 mg : 1 ml. Later, solutions 1 and 2 were mixed by sonification with the volume ratio of 20 : 1 to prepare the $BiVO_4$ precursor solution. The $BiVO_4$-rGO precursor solution was obtained by mixing the prepared $BiVO_4$ precursor solution and GO of desired concentration with sonication. The GO was reduced to rGO during the calcination process to prepare thin films.

3. Preparation of Photocatalyst Thin Films on Substrate

The photocatalyst thin films on substrate were prepared by spin coating method. The prepared precursor solution was dropped on the fluorine doped tin oxide (FTO) glass (1.4×1.4 cm^2 in size, 2 mm in thickness and surface resistivity of ~7 Ω/sq, Aldrich) with various spinning speeds for 45 seconds and a thin layer of precursor solution was prepared on the FTO glass. Then, the coated FTO glass was calcined in furnace at 450 °C for 4 hr. The thickness of photocatalyst precursor solution was controlled by changing the spinning speed. Heterojunction thin films of $WO_3/BiVO_4$ were fabricated by coating the corresponding precursor solutions in series by the same method. To prepare $WO_3/BiVO_4$-rGO films, the $BiVO_4$ precursor solution containing GO was used instead of $BiVO_4$ precursor solution and the GO was transformed to rGO by calcination. The thickness and morphology of thin films were characterized by UHR-SEM (S-4800, Hitachi) and HRXRD (X'Pert PRO MPD, PANalytical) were used to analyze the crystal structure. XPS (K Alpha+, Thermo Scientific) with Al K α radiation in a vacuum chamber ($<5\times10^{-8}$ mbar) was used for confirmation of reduction of GO and thin films for XPS measurement were obtained by spin coating with 500 rpm on the FTO glass using $BiVO_4$ precursor solution dispersed with 10 mg/ml of GO.

4. PEC Performance Measurements of Photocatalyst Thin Films

The photocatalyst thin films prepared on FTO glass were connected with copper wire and used as the working electrode. The exposed surface area of the working electrode was controlled to be 0.5 cm×0.5 cm by using black masking tape. The counter and reference electrodes were the Pt mesh (2.5 cm×2 cm in size, Ametek) and saturated calomel electrode (SCE), respectively. 0.5 M sulfuric acid was used as electrolyte solution in 3 electrodes-photocell. The modulated light was generated from Xe lamp coupled with AM 1.5 filter or monochromator (Mmac-200, Spectro) and was illuminated to photocell connected with potentiostat (VersaSTAT3, Ametek). The potentiostat was used to apply the controlled bias voltage and also to record the photocurrent. The j-V curves were plotted by measuring the photocurrent using AM 1.5 filter with different applied voltages. The incident photon to current conversion efficiency (IPCE) for different wavelengths was calculated for IPCE plot by the equation, IPCE(%)=(1240×photocurrent density)/(wavelength×light irradiance)×100 [26].

RESULTS AND DISCUSSION

1. SEM, XRD, XPS Results

Fig. 1 shows the SEM measurements of $BiVO_4$ and WO_3 thin films on FTO substrate prepared with different spin coating speeds. The thicknesses of $BiVO_4$ thin film were 100 nm and 500 nm for the spin speeds of 500 rpm and 250 rpm, respectively. Because of the higher viscosity of WO_3 precursor solution, the WO_3 thin film was thicker than that of $BiVO_4$ thin film for the same spin coating speeds (the thicknesses of WO_3 thin film were 500 nm and 1 μm for 2,000 rpm and 1,000 rpm, respectively, as shown in Fig. 1(c) and 1(d)). In addition, the WO_3 thin films were composed of nanoparticles of approximately 50 nm, and the $BiVO_4$ thin films were composed of nanoparticles of few hundred nm. Through the SEM images, it was confirmed that the film thickness could be controlled by the change of spin coating speed. The thickness of photocatalyst thin film is one of the important factors to determine

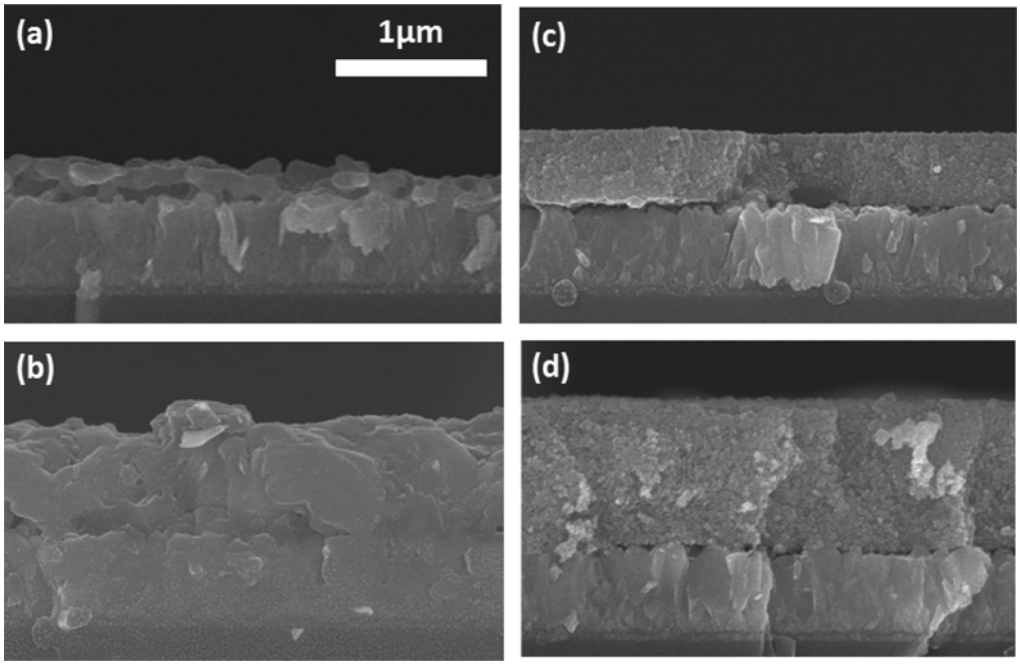

Fig. 1. Cross sectional SEM images (same magnifications) of $BiVO_4$ thin films with spin coating speeds of 500 rpm (a) and 250 rpm (b) and of WO_3 thin films with spin coating speeds of 2,000 rpm (c) and 1,000 rpm (d).

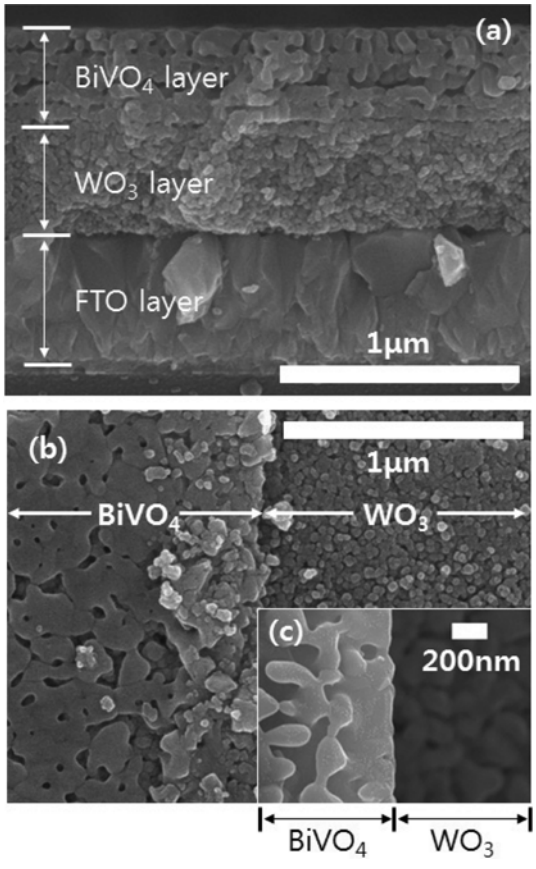

Fig. 2. Cross sectional (a) and top view ((b), (c): different magnifications) SEM images of $WO_3/BiVO_4$ heterojunction thin film with spin speeds of 2,000 rpm for WO_3 and 250 rpm for $BiVO_4$.

the PEC performance.

Fig. 2 shows the SEM images of $WO_3/BiVO_4$ heterojunction thin film, which is composed of WO_3 layer coated on FTO with spin speed of 2,000 rpm and $BiVO_4$ layer coated on WO_3 layer with spin speed of 250 rpm. From the cross sectional view (Fig. 2(a)), the thicknesses of WO_3 and $BiVO_4$ layers are both about 500 nm, while the original thickness of FTO layer is about 600 nm. Fig. 2(b) and 2(c) show the top view SEM images of $BiVO_4$ and WO_3 layers in $WO_3/BiVO_4$ heterojunction, where the whole FTO substrate was first coated with WO_3 layer and, later, just one-half of WO_3 layer was coated with $BiVO_4$ layer by masking the other half with adhesive tape (Scotch Magic Tape, 3M) during spin coating. The top views of heterojunction thin film here also show the differences of nanoparticle size and compactness for both WO_3 and $BiVO_4$ layers.

The XRD patterns of $BiVO_4$, WO_3 and $WO_3/BiVO_4$ thin films coated on FTO glass are shown in Fig. 3. The structures of monoclinic $BiVO_4$ (#00-005-0363) and monoclinic WO_3 (#01-075-1866) were confirmed in Figs. 3(a) and 3(b). The characteristic peaks of both $BiVO_4$ and WO_3 were observed in the XRD pattern of $WO_3/BiVO_4$ heterojunction thin films in Fig. 3(c). The monoclinic system is known as the best crystal system for PEC water splitting in both WO_3 and $BiVO_4$ [27-29].

For the $WO_3/BiVO_4$-rGO heterojunction thin films, the GO or rGO could not be observed by XRD measurement because of the small amount of GO in $BiVO_4$ layer [6]. Instead, C1s XPS measurements before and after calcination were used to confirm the reduction of GO included in $BiVO_4$-rGO photocatalyst layer. Fig. 4 shows the C1s XPS spectra of $BiVO_4$ thin film containing GO before and after calcination. The binding energy to show the C-O bonding peak of $BiVO_4$-GO film in the range of about 286-287 eV

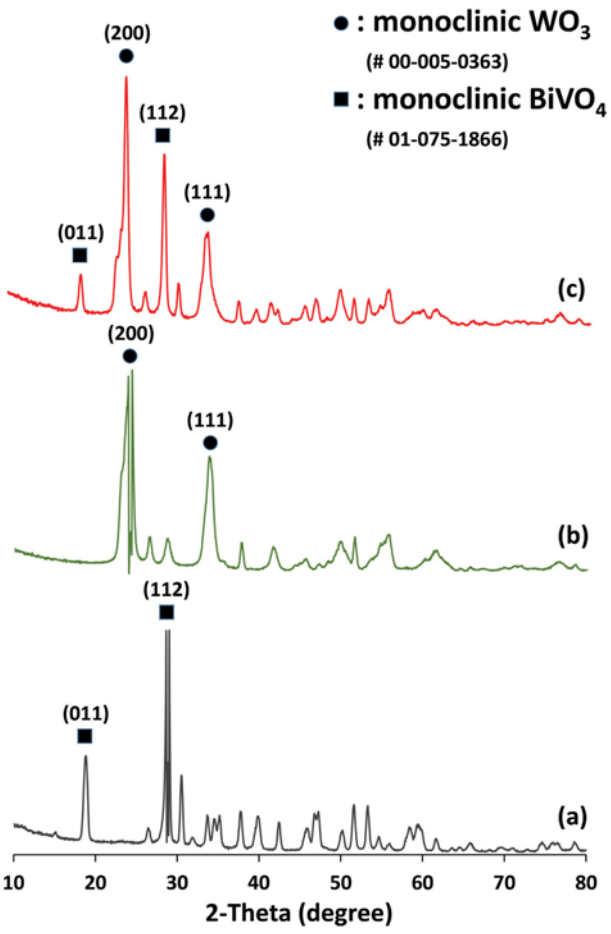

Fig. 3. XRD patterns of $BiVO_4$ (a), WO_3 (b) and $WO_3/BiVO_4$ (c) thin films coated on FTO glass.

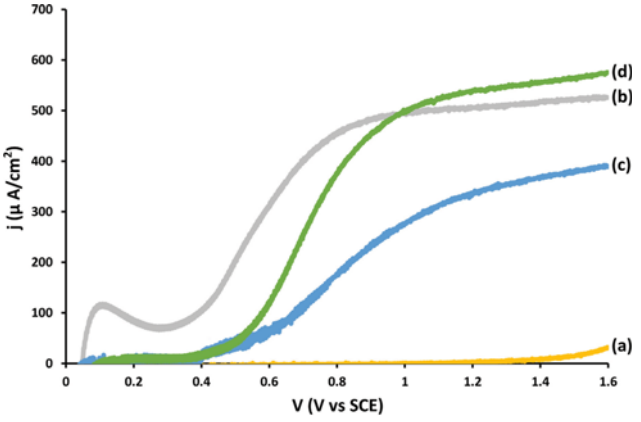

Fig. 5. j-V curves of $BiVO_4$ film (a), WO_3 film (b) and $WO_3/BiVO_4$ heterojunction films with different thicknesses ((c): 1 μm WO_3+100 nm $BiVO_4$, (d): 500 nm WO_3+100 nm $BiVO_4$).

decreased after calcination, while the C-C bonding peak in 285 eV and C(O)O bonding peak in 288 eV do not change (Fig. 4(b)). It indicates that the oxygen in functional group of GO was vaporized and removed selectively by calcination [25,30]. The reduction of GO will lead to the improvement of electrical property, but, in this study, all the functional groups were not removed by calcination, and the remaining functional groups can have a negative effect on photocatalytic activity. The calcination of $WO_3/BiVO_4$-GO coated on FTO glass caused not only the crystallization of $BiVO_4$ but also the reduction of GO from the results of XRD and XPS.

2. PEC Performances of Photocatalyst Thin Films

Fig. 5 shows the j-V curves of $BiVO_4$, WO_3 and $WO_3/BiVO_4$ heterojunction films prepared in this study. The $BiVO_4$ thin film with thickness of 500 nm produced lower photocurrent density with maximum of about 30 μA/cm^2, while the WO_3 thin film of 1 μm produced higher photocurrent density with maximum photocurrent density of 525 μA/cm^2 (Figs. 5(a) and 5(b)). The $BiVO_4$ can absorb broader range of visible light than WO_3 due to narrower band gap [31], but the photocurrent density generated by WO_3 thin film was higher than $BiVO_4$ thin film, because bare $BiVO_4$ has a higher recombination rate than WO_3 [6]. The $WO_3/BiVO_4$ heterojunction thin films can be used to obtain both advantages of $BiVO_4$ and WO_3 layers. The backside illumination showed the higher efficiency than front illumination for heterojunction thin films, because input light can be utilized more efficiently [18]. The PEC performance of $WO_3/BiVO_4$ heterojunction film was measured with backside illumination in this study. However, for the thickness of 1 μm WO_3 layer, the photocurrent generated by the $WO_3/BiVO_4$ heterojunction thin film was lower than by bare WO_3

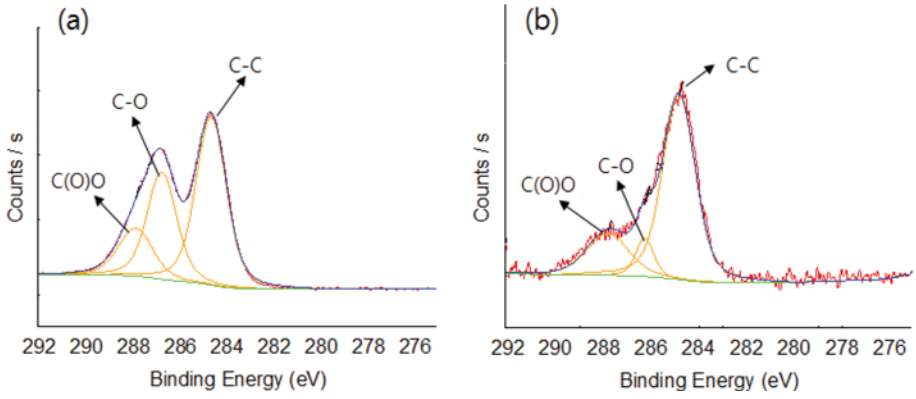

Fig. 4. C1s XPS spectra of $BiVO_4$ thin film containing GO before (a) and after (b) calcination.

thin film (Fig. 5(c)), because most of the input light was absorbed in thick WO_3 bottom layer and the photogenerated electrons and holes in thick WO_3 layer disappeared by significant recombination reaction and also because the $BiVO_4$ layer has poor transfer property for electron holes. For the WO_3 film thickness of 500 nm, the photocurrent density of $WO_3/BiVO_4$ heterojunction thin film was slightly higher than bare WO_3 layer. Some electron-hole pairs were photogenerated in $BiVO_4$ layer, because some input light could pass through the thinner WO_3 layer, and they could be transferred to reaction sites successfully in heterojunction thin film (Fig. 5(d)).

In this case, however, the improvement of PEC performance for $WO_3/BiVO_4$ heterojunction thin film was not notable due to poor electrical property of $BiVO_4$. To overcome these problems, rGO was added to the $BiVO_4$ layer. The PEC performance of $WO_3/BiVO_4$-rGO films with GO concentration of about 2 mg/ml in precursor solution was compared with that of $WO_3/BiVO_4$ film in Fig. 6. Because $BiVO_4$ has the poor electrical conductivity and rGO has the higher electrical conductivity, the photoelectrons generated in $BiVO_4$-rGO layer can be transferred [6] to the WO_3 layer

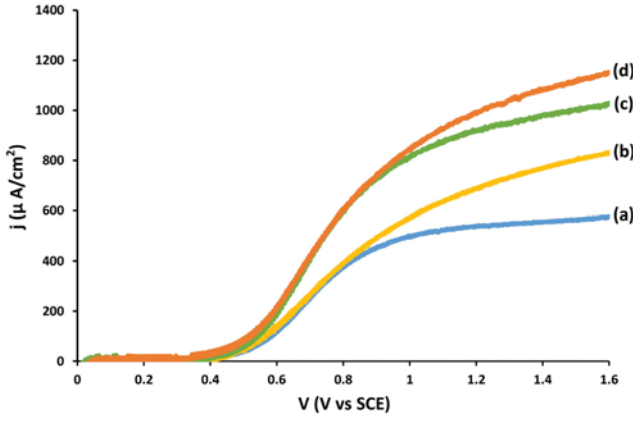

Fig. 6. j-V curves of $WO_3/BiVO_4$ film (a) and $WO_3/BiVO_4$-rGO films with different thicknesses of $BiVO_4$-rGO layer ((b) 50 nm, (c) 100 nm and (d) 500 nm). The WO_3 layer thickness was 500 nm.

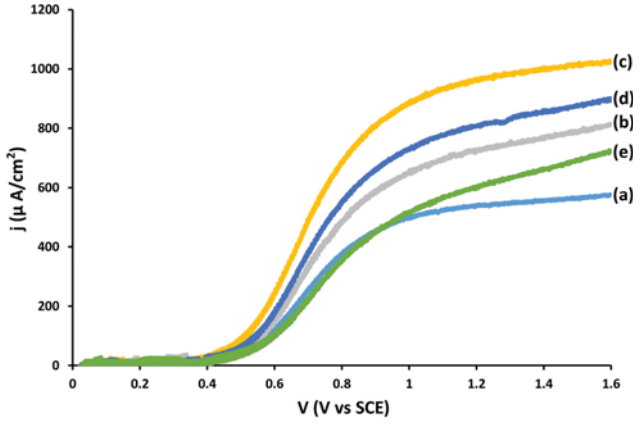

Fig. 7. Comparison of j-V curves in $WO_3/BiVO_4$-rGO heterojunction films with different concentrations of rGO (rGO concentration, (a) 0, (b) 1, (c) 2, (d) 3 and (e) 4 mg/ml).

much faster and the $WO_3/BiVO_4$-rGO heterojunction thin film can produce higher photocurrent density. The higher the thickness of $BiVO_4$-rGO layer was, the better the PEC performance was, because of the higher absorption of light in $BiVO_4$-rGO layer for the range of $BiVO_4$-rGO layer thickness in this study.

Fig. 7 shows the j-V curves of $WO_3/BiVO_4$-rGO heterojunction films prepared with different concentrations of GO. Initially, the photocurrent density increased with the increase of rGO concentration, reached the maximum and finally decreased. The best performance of PEC measurement in our experiments was observed with the GO concentration of 2 mg/ml. At low rGO concentration, the enhancement of electrical conductivity by rGO was not high enough and the photocurrent generation was low. If the rGO concentration is too high, a significant amount of light can be absorbed by the rGO instead of photocatalyst, and the number of photogenerated electron-hole pairs decreases and the photocurrent density also decreases.

The IPCE plots for WO_3, $WO_3/BiVO_4$ and $WO_3/BiVO_4$-rGO thin films are compared in Fig. 8. The thicknesses of those thin films were selected for the conditions to show the best performance in this study. The PEC performance can be enhanced by the $WO_3/BiVO_4$ heterojunction and even more by the $WO_3/BiVO_4$-rGO heterojunction structure. The WO_3 thin film showed the maximum IPCE of about 11% at 360 nm wavelength and could not generate the photocurrent at the wavelength higher than 470 nm. For $WO_3/BiVO_4$ film, the maximum IPCE was similar with WO_3 film, but light of wider wavelength could be used to produce photocurrent. On the other hand, the IPCE in $WO_3/BiVO_4$-rGO film was more than 16% for the wavelength of at 410-440 nm and showed the relatively higher efficiencies for all wavelengths longer than 380 nm. This result confirmed that the $WO_3/BiVO_4$-rGO heterojunction thin film could utilize sunlight more efficiently for wide wavelength region and generate more photogenerated electron-hole pairs.

CONCLUSION

Precursor solutions for WO_3 and $BiVO_4$ photocatalysts were synthesized by solution processes. The GO was prepared and was

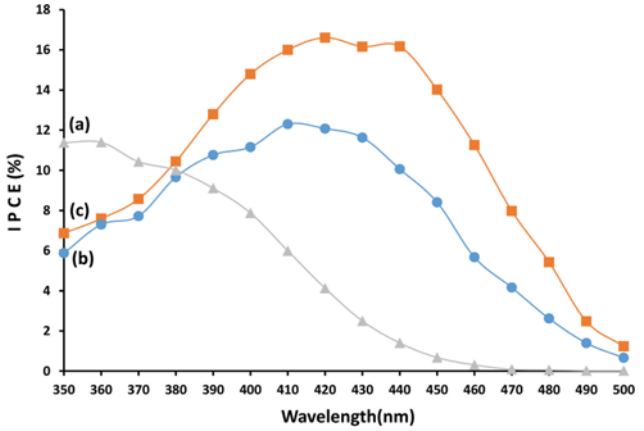

Fig. 8. IPCE plots (applied voltage V vs SCE=1 V) of highest PEC performance with different films ((a) WO_3 film, (b) $WO_3/BiVO_4$ film and (c) $WO_3/BiVO_4$-rGO film) in this study.

added into the $BiVO_4$ precursor solution. The photocatalyst thin films of WO_3 and $BiVO_4$, $WO_3/BiVO_4$ and $WO_3/BiVO_4$-rGO on FTO glass were prepared from precursor solutions by spin coating and calcination processes for the first time, and the PEC performance of prepared photocatalyst thin films was analyzed systematically. The $WO_3/BiVO_4$ heterojunction layer with controlled film thicknesses showed better PEC performance than the bare WO_3 or $BiVO_4$ layer. The electrical conductivity of $BiVO_4$ layer was enhanced significantly by adding rGO, and the $WO_3/BiVO_4$-rGO film showed a noticeable increase in photocurrent density, and the optimum concentration of rGO in this study was 2 mg/ml. The best photocurrent density of $WO_3/BiVO_4$-rGO film in this study was about 1.1 mA/cm^2 and was far better than those of $BiVO_4$ and WO_3 single thin films, which were about 30 $\mu A/cm^2$ and 525 $\mu A/cm^2$, respectively. These photocurrent densities in this study are not enough for practical application, but the synergistic effect of $WO_3/BiVO_4$ heterojunction and $BiVO_4$-rGO composite film was confirmed for the first time. Therefore, the photocatalytic activity of the $WO_3/BiVO_4$-rGO film is still expected to increase more by optimizing the layer thickness and also by improving the quality of graphene. This study suggests that the rGO combined with some composite heterojunction films can be used to increase the efficiency of photoanode.

ACKNOWLEDGEMENTS

This work (grant number NRF-2016R1A2B4008876) was supported by Mid-career Researcher Program through NRF funded by the MSIP. Instrumental analysis was supported from the central laboratory of Kangwon National University.

REFERENCES

1. R. Van De Krol, Y. Liang and J. Schoonman, *J. Mater. Chem.*, **18**, 2311 (2008).
2. X. Liu, F. Wang and Q. Wang, *Phys. Chem. Chem. Phys.*, **14**, 7894 (2012).
3. G. R. Bamwenda and H. Arakawa, *Appl. Catal. A Gen.*, **210**, 181 (2001).
4. F. Wang, C. Di Valentin and G. Pacchioni, *J. Phys. Chem. C.*, **116**, 8901 (2012).
5. T. Hisatomi, J. Kubota and K. Domen, *Chem. Soc. Rev.*, **43**, 7520 (2014).
6. Y. H. Ng, A. Iwase, A. Kudo and R. Amal, *J. Phys. Chem. Lett.*, **1**, 2607 (2010).
7. P. Pathak, S. Gupta, K. Grosulak, H. Imahori and V. Subramanian, *J. Phys. Chem. C.*, **119**, 7543 (2015).
8. J. Ding and K.-S. Kim, *AIChE J.*, **62**, 421 (2016).
9. J. Y. Kim, G. Magesh, D. H. Youn, J.-W. Jang, J. Kubota, K. Domen and J. S. Lee, *Sci. Rep.*, **3**, 1 (2013).
10. Z. Qin, H. Tian, T. Su, H. Ji and Z. Guo, *RSC Adv.*, **6**, 52665 (2016).
11. T. Su, H. Tian, Z. Qin and H. Ji, *Appl. Catal. B.*, **202**, 364 (2017).
12. A. Zaleska, *Recent Patents Eng.*, **2**, 157 (2008).
13. S. J. A. Moniz, S. A. Shevlin, D. J. Martin, Z.-X. Guo and J. Tang, *Energy Environ. Sci.*, **8**, 731 (2015).
14. H. Wang, L. Zhang, Z. Chen, J. Hu, S. Li, Z. Wang, J. Liu and X. Wang, *Chem. Soc. Rev.*, **43**, 5234 (2014).
15. J. Low, J. Yu, M. Jaroniec, S. Wageh and A. A. Al-Ghamdi, *Adv. Mater.*, **29**, 1 (2017).
16. P. Chatchai, Y. Murakami, S. Kishioka, A. Y. Nosaka and Y. Nosaka, *Electrochim. Acta*, **54**, 1147 (2009).
17. P. Chatchai, S. Kishioka, Y. Murakami, A. Y. Nosaka and Y. Nosaka, *Electrochim. Acta*, **55**, 592 (2010).
18. J. Su, L. Guo, N. Bao and C. A. Grimes, *Nano Lett.*, **11**, 1928 (2011).
19. S. J. Hong, S. Lee, J. S. Jang and J. S. Lee, *Energy Environ. Sci.*, **4**, 1781 (2011).
20. N. J. Bell, Y. H. Ng, A. Du, H. Coster, S. C. Smith and R. Amal, *J. Phys. Chem. C.*, **115**, 6004 (2011).
21. Q. P. Luo, X. Y. Yu, B. X. Lei, H. Y. Chen, D. Bin Kuang and C. Y. Su, *J. Phys. Chem. C.*, **116**, 8111 (2012).
22. J. Guo, Y. Li, S. Zhu, Z. Chen, Q. Liu, D. Zhang, W.-J. Moon and D.-M. Song, *RSC Adv.*, **2**, 1356 (2012).
23. F. K. Meng, J. T. Li, S. K. Cushing, J. Bright, M. J. Zhi, J. D. Rowley, Z. L. Hong, A. Manivannan, A. D. Bristow and N. Q. Wu, *Acs Catal.*, **3**, 746 (2013).
24. A. K. Geim and K. S. Novoselov, *Nat. Mater.*, **6**, 183 (2007).
25. D. C. Marcano, D. V. Kosynkin, J. M. Berlin, A. Sinitskii, Z. Sun, A. Slesarev, L. B. Alemany, W. Lu and J. M. Tour, *ACS Nano.*, **4**, 4806 (2010).
26. S. K. Biswas, J.-O. Baeg, S.-J. Moon, K. Kong and W.-W. So, *J. Nanoparticle Res.*, **14**, 667 (2012).
27. H. Zhang, J. Yang, D. Li, W. Guo, Q. Qin, L. Zhu and W. Zheng, *Appl. Surf. Sci.*, **305**, 274 (2014).
28. A. Kudo, K. Omori and H. Kato, *J. Am. Chem. Soc.*, **121**, 11459 (1999).
29. P. Dong, X. Xi, X. Zhang, G. Hou and R. Guan, *Materials*, **9** (2016).
30. N. M. Huang, H. N. Lim, C. H. Chia, M. a. Yarmo and M. R. Muhamad, *Int. J. Nanomedicine.*, **6**, 3443 (2011).
31. K. Sayama, A. Nomura, T. Arai, T. Sugita, R. Abe, M. Yanagida, T. Oi, Y. Iwasaki, Y. Abe and H. Sugihara, *J. Phys. Chem. B.*, **11352**, 110 (2006).